Reliability-based hull geometry optimisation of a point-absorber wave energy converter with power take-off structural reliability objectives

Received: 1 March 2021 | Revised: 22 June 2021 | Accepted: 8 July 2021

DOI: 10.1049/rpg2.12249

IET Renewable Power Generation

The Institution of Engineering and Technology WILEY

ORIGINAL RESEARCH PAPER

Reliability-based hull geometry optimisation of a point-absorber wave energy converter with power take-off structural reliability objectives

Anna Garcia-Teruel[1] | **Caitlyn E. Clark**[2]

[1] Institute for Energy Systems, School of Engineering, The University of Edinburgh, Edinburgh, UK

[2] National Renewable Energy Laboratory, Golden, Colorado, USA

Correspondence
Anna Garcia-Teruel, Institute for Energy Systems, School of Engineering, The University of Edinburgh, Edinburgh, UK.
Email: a.garcia-teruel@ed.ac.uk; caitlyn.clark@nrel.gov

Abstract

Recent studies have focused on optimising wave energy converter (WEC) designs, maximising their power performance and techno-economic feasibility. Reliability has yet to be fully considered in these formulations, despite its impact on cost and performance. In this study, this gap is addressed by developing a reliability-based design optimisation framework for WEC hull geometries to explore the trade-off between power performance and power take-off (PTO) system damage equivalent loading (DEL). Optimised hull geometries for two sites are considered (from the centre of the North Sea and off the west coast of Norway), and two directions of motions (heave and surge). Results indicate that site characteristics affect the potential power production and DEL for an optimal WEC design. These are also affected by the direction of motion for power extraction, which also significantly changes optimal hull shape characteristics. Optimal surging WEC designs have edges facing oncoming wave directions, while heaving WECs have pointed bottoms, both to streamline movement. Larger, more convex WECs result in greater power production and DEL, while smaller, more concave WECs result in lesser power production and DEL. These findings underline the importance of considering WEC hull geometry in early design processes to optimise cost, power production, and reliability.

1 | INTRODUCTION

Wave energy is abundant, geographically diverse, predictable, and complimentary to other energy resources [1]. Its potential to provide plentiful, reliable, and renewable energy to coastal communities across the world has driven interest from governments, researchers, educators, investors, and developers in building a sector around this energy conversion technology [2]. However, major technical hurdles still bar wave energy conversion technologies from being realised to their full commercial potential. A successful transition from a nascent technology to a competitive, commercial proposition requires addressing these technical hurdles so that wave energy conversion technologies can produce efficient, reliable electricity.

As wave energy converter (WEC) developers continue to demonstrate their device's ability to produce energy and the industry progresses towards commercialisation, ensuring adequate reliability is becoming increasingly important. Issues with reliability and survivability of WEC designs have previously led to setbacks for private developers including closure and delayed or limited testing of devices [3]. Ultimately, the reliability of these devices will affect capital costs (via design requirements for reliability), operational costs (via maintenance and repair required to operate), and power production (via downtime). Low accessibility and availability of spare parts and the need for specially-trained technicians will only exacerbate the impacts of low reliability. Designing WECs to withstand and produce energy in highly energetic marine environments without over-engineering their design is fundamental to enabling their implementation, and overcoming their development and commercial challenges.

The importance of considering WEC reliability in early design phases is underlined by its inherent relationship with power production. Producing energy in highly energetic sea

states increases revenue potential, as well as loads that the WEC must withstand and capital costs involved with ensuring that reliability through design and manufacturing. Considering this design trade-off between power production and component reliability throughout the WEC design process could improve technology readiness. Particularly in device geometry design, there is an opportunity to reduce structural and PTO loads [3]. Optimising WEC shape for reliability and power could decrease downtime and required maintenance costs, and help ensure that WECs perform as they were designed for their intended lifespan.

1.1 | Previous work

Until recently, research integrating reliability into WEC design has been limited, instead focusing on WEC optimisation for power production or reduced capital expenditures. This review focuses on the most relevant previous work pertaining to reliability-based geometry optimisation of WECs, addressing: (1) WEC hull geometry optimisation for cost and power production, (2) reliability-based design optimisation of WEC foundations, and (3) WEC hull geometry effects on varying component loads. These bodies of research provide the necessary theory and methods to relate component reliability to WEC hull geometry optimisation. For more information on how reliability information is and can be integrated into structural and mechanical design and analysis of WECs, refer to Ref. [4–7].

WEC hulls have been extensively studied in the past decade, with a focus on evaluating different WEC hull geometries and their impact on performance, as reported in [8]. Most studies focus on maximising annual energy production and consider costs only through a scaling approach, wherein cost is scaled with device size. This major assumption of scaled costs is a result of (1) sparse cost information being available at early design stages, and (2) optimisation algorithms requiring efficient, often simplified analytical cost models to minimise computational expense during objective function evaluations. Additionally, most geometry optimisation studies are based on simple shape definitions such as vertical cylinders or spheres. A more adaptable method able of generating diverse shapes was developed by McCabe et al. [9, 10], which employs bi-cubic B-spline surfaces to represent the submerged hull. This approach was expanded by Garcia-Teruel et al. to be applicable in multiple degrees-of-freedom [11] and to ensure robustness of the method for a number of applications [12]. In these latter studies, costs were represented through the hull's submerged surface area and submerged volume, but reliability was not considered.

Initial work considering reliability in the optimisation of WEC hulls was introduced by Kurniawan et al. in [13]. In that study, the reactive force on the hinge of an oscillating surge WEC was included in one of the objective functions. However, work in this area is often limited by the computational expense of integrating component force calculations and reliability estimation into an optimisation scheme. Focusing on structural components through reliability-based design optimisation (RBDO) techniques, Ambuhl et al. optimised pile and foundation structural parameters for the WaveStar device given four failure modes (bending, overturning, sliding, and bearing capacity failures). The failure surfaces were incorporated into their structural constraints to maximise profitability [5]. Ambuhl et al. then identify and model fatigue failure as a critical failure mode, identifying welded and bolted joints to be particularly vulnerable to failure due to these structural details experiencing high stress concentrations [14]. In each of these studies, failure is considered as a constraint. Reliability has also been considered in mechanical components of WECs. Yang et al. focused on the power take-off (PTO) of a point absorber-type WEC, like the current study. Whereas the current work focuses on the structural modelling and analysis of the welded joint between the hull and the piston cylinder (similar to Ambuhl et al. [5]), Yang et al. model the wear of the piston ring by the piston cylinder using an abrasion modelling approach [15]. Although they only consider one sea state, Yang et al. develop methods to address component failure in a PTO system, a major contribution of their study.

A number of studies have also investigated structural integrity of WECs considering the impacts of hull geometry. Studies that consider loads for the device design (rather than reliability), include for example, the development of an oscillating wave surge converter (OWSC) composed of various controllable flaps with the aim of maximising power and reducing design loads through geometry control by Tom et al. [16]; or the consideration of the pressure distribution on the device's surface to estimate the device's required mass so that the device withstands wave loading for three OWSC configurations by Yu et al. [17]. Other studies have used numerical methods to study hydrodynamic loads on different shapes [18] and how to represent extreme structural and design loads for WECs [19–21]. Beirao et al. [18] studied the effect of WEC hull geometry on the loads on the supporting cables and PTO cylinder rod of a heaving point absorber. They considered three geometries: a sphere, a horizontal cylinder, and a vertical cylinder with a conical bottom. The results showed that a partially submerged buoy experienced the greatest stresses and excursion if compared to a fully submerged buoy or a buoy floating at the surface. Overall, the sphere showed the lowest stress values. Additionally, the loads depending on the piston position were compared, which were found to be highest in the cables, when the piston was retracted. When the piston was extended, both the rod and cables were identified as critical components. Van Rij et al. [22] investigated the PTO damage equivalent loads (DELs) for point absorber type devices. In that study, two floater geometries (a vertical cylinder with truncated conical bottom and a rhombus) and two mooring configurations (a monopile and a spar-plate configuration) were considered. Drag coefficients were then obtained using a computational fluid dynamics model, and PTO force data were generated with a time-domain model implemented in WEC-Sim [23]. The rhombus-shaped floater with a spar-plate mooring configuration resulted in the lowest fatigue loads. These studies inform the understanding of how WEC hull geometry is related to the reliability of different components. The PTO was identified as a critical component in

these previous studies. However, the employed finite-element and computational fluid dynamics models are too computationally demanding to be used within an optimisation process. Building on this, a first step towards developing a suitable method for considering PTO reliability in a WEC hull geometry optimisation problem was introduced by Clark et al. [24]. This approach characterises PTO reliability by means of damage equivalent loads (DELs) at the PTO rod connection point. This approach will be leveraged in the present study to incorporate reliability considerations in the geometry optimisation process.

1.2 | Research objective

The previous literature has enabled the current work, which addresses the opportunity to implement reliability-based design optimisation of hull geometries to design more optimal WECs. This would allow for hull geometries with advantageous reliability scores to be prioritised, balancing cost, power production, and reliability objectives. In a previous study conducted by the authors, a method for estimating reliability of a WEC PTO was established, and preliminary results proving the importance of hull geometry on power production and PTO reliability were obtained by comparing three static, non-optimal shapes [24]. The main goal of this study is to integrate the previously developed method of reliability analysis into an optimisation framework to generate improved WEC hull geometries considering reliability and power production as objectives.

This is achieved by applying an adaptable geometry optimisation framework capable of generating improved and diverse WEC hull geometries [10, 12, 25]. Within this framework, a hydrodynamic analysis is performed to provide power production and PTO-forces for each geometry [11, 24]. Based on the generated PTO-force time series, we use Rainflow counting and appropriate *S–N* curves to count the number of fatigue cycles and relate it to damage equivalent load (DEL) metrics. The generated optimal shapes are compared with the simple shapes analysed in [24] for the development of the reliability assessment method. This allows for the comparison of several hull shapes and their resulting PTO damage and demonstrates the ability of the optimisation approach to generate optimal shapes with improved reliability characteristics.

This study is divided into three sections. First, the methodology is described in Section 2, which (1) defines the case studies, met-ocean conditions, and WEC system characteristics, (2) describes the hydrodynamic model used to determine the PTO-force time series for each case, (3) details the fatigue DEL calculation based on that PTO-force time series, and (4) briefly describes the optimisation method. The results for the reliability-based optimisation are then discussed based on (1) the achieved objective function values, and (2) on the resulting optimal shapes in Section 3. Conclusions and future work follow in Section 4.

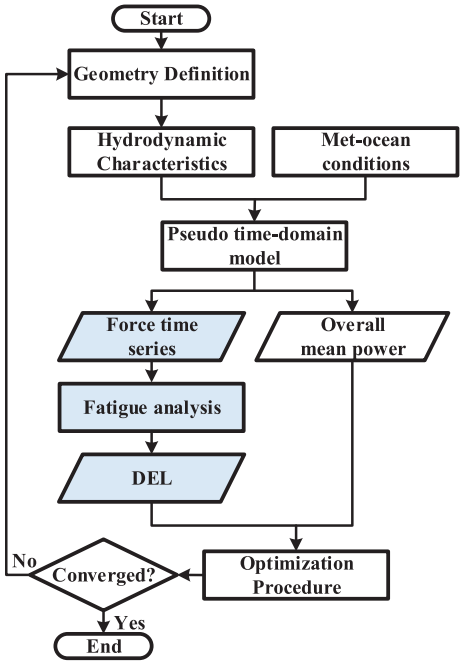

FIGURE 1 Flow chart to provide overview of optimisation process. The reliability metric calculation is highlighted in blue

2 | METHODOLOGY

This section details the methods developed and used for the reliability analysis and optimisation of the WEC hull geometry. An overview of the used method is provided in Figure 1. To include reliability-based considerations in the optimisation process, a multi-objective optimisation approach was used, aiming to minimise the DEL experienced at the PTO rod weld, while maximising the overall mean power. Optimal WEC hull geometries are generated considering two energy absorption modes, and two geographic locations. We introduce the main characteristics of the WEC-system and the geometry definition in Section 2.1. Section 2.2 details the considered met-ocean conditions, followed by the hydrodynamic model description in Section 2.3. Section 2.4 describes the fatigue analysis methods. Finally, a brief description of the optimisation methodology is provided in Section 2.5.

2.1 | WEC system and hull geometry definition

In this study, we analyse a point absorber type WEC oscillating in a single mode of motion (either heave or surge). The WEC floater reacts against a PTO, such as a linear generator or a hydraulic piston, fixed (1) perpendicular to the sea bed, or (2) perpendicular to some vertical surface in the water column (see Figure 2). We assume the PTO system is composed of a moving rod welded to the floating body and a fixed component. The geometry is defined so that diverse shapes can be generated through the optimisation approach introduced by McCabe

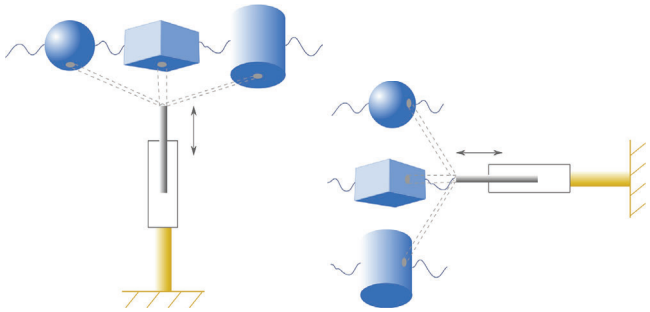

FIGURE 2 Schematic representation of the WEC systems oscillating in (a) heave and (b) surge [24]

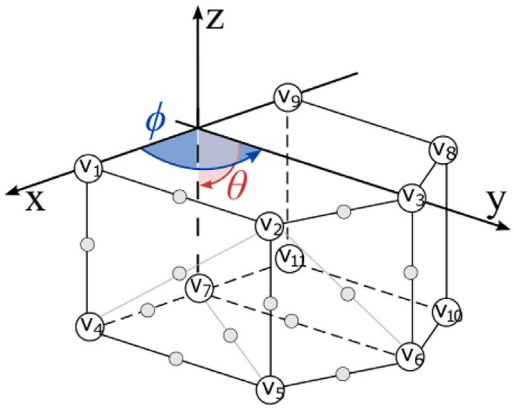

FIGURE 3 Polyhedron with numbered vertices v_n and example representations of the interpolated control points in grey [26]

et al. [10]. The results of the optimisation are compared to a static non-optimised barge shape with dimensions chosen so that its draft (10 m) and characteristic width (20 m) are comparable to the generated, optimal hull shapes.

With the approach introduced by McCabe et al. [10] the WEC hull geometries are defined based on a polyhedron symmetrical along the x–z plane. The corner points are used as vertices v_n, between which further control points are defined through interpolation (Figure 3). The control points are then approximated by a bi-cubic B-spline surface. Some of the vertices' coordinates are fixed, since the vertices lie on the free surface or on the symmetry plane, but the rest (a total of 22 coordinates) make up the genotype of the genetic algorithm introduced in Section 2.5, and can be changed randomly within defined ranges. Note that vertices' coordinates are defined within a spherical coordinate system (r_n, ϕ_n, θ_n).

Constraints are instituted to maintain physically possible shapes. Radial coordinates, r_n are constrained by:

$$2.5\ \text{m} \leq r_n \leq 12.5\ \text{m}.$$

Azimuth angles are constrained by:

$$\frac{\pi}{16} \leq \phi_n \leq \frac{15\pi}{16} \quad \text{for} \quad n = 2, 3, 5, 6, 8, 10;$$

$$\frac{\pi}{16} \leq \phi_n \leq \frac{\pi}{2} \quad \text{for} \quad n = 2, 5;$$

$$\frac{\pi}{2} \leq \phi_n \leq \frac{15\pi}{16} \quad \text{for} \quad n = 8, 10;$$

$$\text{with } \phi_2 \leq \phi_3 \leq \phi_8;$$

$$\text{and } \phi_5 \leq \phi_6 \leq \phi_{10}.$$

Zenith angles (measured from the $z = 0$) are constrained by:

$$\frac{\pi}{16} \leq \theta_n \leq \frac{7\pi}{16} \quad \text{for} \quad n = 4, 5, 6, 10, 11.$$

Additional constraints needed to be included to ensure robustness of the method; these constraints are detailed by Garcia-Teruel et al. [12].

TABLE 1 Site characteristics

	North Sea	Norway
Location	55.13N, 3.43E	61.85N, 4.23E
Water depth (m)	29	200
Distance to shore (km)	300	30
Mean wave power density (kW/m)	14.29	46.43
50-year U_w at 10 m (m/s)	27.2	33.49
50-year H_s (m)	8.66	10.96
Mean value of T_p (s)	6.93	11.06

2.2 | Met-ocean conditions of the studied geographic locations

To generate the sea state conditions experienced by the WEC, we considered two geographic locations, one in the central North Sea, and the other off the southwestern coast of Norway, which correspond to Site 15 and Site 14, respectively, of the European Union's MARINA Project [27]. They were chosen to allow for comparison of the WEC response in two distinct site conditions. These site conditions are described in Table 1.

To model the sea states of the two locations, we first derived the characteristic sea states at each location, and then used the resulting significant wave height H_s, peak period T_p, and probability of occurrence as input for the hydrodynamic model. The marginal and joint distributions used in this study are obtained by fitting analytic solutions to raw data and are characterised by 1-h mean wind speed at ten meters above mean sea level (U_w), significant wave height (H_s) and spectral peak period (T_p) [28]. The joint probability density function (PDF) of U_w, H_s, and T_p is defined by the marginal PDF of U_w (f_{U_w}), the PDF of H_s conditional on U_w ($f_{H_s|U_w}$) and the PDF of T_p conditional on H_s ($f_{T_p|H_s}$). The parameters and equations that define these distributions can be found in the original description of the site conditions [28]. The resulting representative sea states are described in Tables 2 and 3 in the appendix. For the purposes of this study,

we assume the waves are unidirectional, approaching the WEC from the west.

2.3 | Hydrodynamic model

The hydrodynamic model used in this study is based on linear wave theory, where wave height is assumed to be much smaller than wave length and water depth, and oscillations are assumed to be small. In this case, waves are represented as harmonic oscillations of different wave height and frequency, which can be linearly superposed to represent an irregular sea. For each sea state the relation of wave amplitude to frequency is defined by a Bretschneider spectrum, where 150 frequencies (ω_k) from 0 to 3 rad/s in $\Delta\omega = 0.02$ steps are analysed.

WAMIT [29] –a frequency-domain program based on a boundary element method (BEM)– is used to calculate the hydrodynamic characteristics for each shape based on the frequencies selected to represent the wave spectrum. The hydrodynamic characteristics for each shape, are then used within the hydrodynamic model, which can be described as a pseudo time-domain model. That is a frequency-domain model, in which the oscillation time series is calculated to be able to apply PTO rating and stroke constraints to the power production calculation [8, 11].

To introduce all forces considered in the equation of motion of the WEC under these assumptions, the equation is introduced in (1). The main forces affecting the motion are the wave excitation force $\mathbf{F}_e$, the PTO-force $\mathbf{F}_{PTO}$, the WEC inertia $\mathbf{M}$, the radiation force composed of an added mass $\mathbf{M}_{rad}$ and a radiation damping $\mathbf{C}_{rad}$ terms, and the hydrostatic force represented by a stiffness term $\mathbf{K}_H$ following the Archimedes principle. An additional damping term $\mathbf{C}_{loss}$ is included to represent friction losses as done in [10]. This is a diagonal matrix where for each mode of motion (i) friction losses are represented as 10% of the maximal value of $C_{rad}(i, j)$ for $j = i$ found across all wave frequencies. The stiffness value from the mooring lines is neglected, because it is considered to be much smaller than the hydrostatic stiffness value.

$$\hat{\mathbf{F}}_e + \hat{\mathbf{F}}_{PTO} = \left[-\omega^2(\mathbf{M} + \mathbf{M}_{rad}) + i\omega(\mathbf{C}_{rad} + \mathbf{C}_{loss}) + \mathbf{K}_H\right]\hat{\mathbf{X}}(\omega_k) \tag{1}$$

$\hat{\mathbf{X}}(\omega)$ represents the complex amplitude of oscillation that can be understood as the Fourier transform of the of the device position $\mathbf{x}(t)$, and is a 6×1 column vector if considering the six modes of motion i.

The oscillation time series can then be obtained for each mode of motion i, sea state s and set q of random phase shifts $\psi_{s,k,q}$ from the superposition of the single harmonic oscillation representations at each frequency ω_k. This is given by

$$x_{s,q,i}(t) = \sum_{k=1}^{n_k} \left(\hat{X}_{s,i}(\omega_k)\cos(\omega_k t + \psi_{s,k,q} + \angle\hat{X}_{s,i}(\omega_k)\right) \quad \text{for} \quad s = 1, .., n_s, q = 1, .., 10, i = 1, \dots, 6. \tag{2}$$

with $n_k = 150$ frequencies. Note that the total number of sea states, n_s, will vary for the two sites considered within this study. This same concept of building a times series from a frequency-domain analysis is used for the PTO force time series, which will be introduced in the following sub-sections.

It should be noted that non-linear effects are not considered when using this method. This could lead to both under- or over-estimation of the experienced forces. However, Barbarit et al. reported in [30], that linear theory tends to overestimate the WEC dynamic response and absorbed power. With the purpose of developing a method suitable for hull geometry optimisation at early design stages, the considered assumptions seem reasonable to provide upper limits of the system performance, while taking into account PTO-reliability.

2.3.1 | Overall mean power estimation

The overall mean power is used to describe the device's power performance. For this purpose, an idealised semi-optimal control strategy is assumed, which sets the mass, damping and stiffness terms composing the PTO-force to match the impedance $\mathbf{Z}$ of the device at the energy period $T_e = 2\pi/\omega_e$ (see Equation (3)). Here $\hat{\mathbf{U}}$ represents a vector of complex amplitudes of the oscillation velocity in six degrees of freedom, and $\hat{\mathbf{X}}$ is the corresponding vector of complex amplitudes of oscillation.

$$\hat{\mathbf{F}}_e = \mathbf{Z}\hat{\mathbf{U}} = \mathbf{Z}i\omega\hat{\mathbf{X}} \tag{3}$$

The instantaneous available power at a given sea state is calculated with the help of the oscillation velocity time series - if the maximum PTO stroke x_{MAX} and PTO rating $P_{PTO,MAX}$ are not exceeded, such that

$$P_{U,s,q}(t) = \dot{\mathbf{x}}_{s,q}^T(t)[\mathbf{C}_{rad}(\omega_e) + \mathbf{C}_{loss}]\dot{\mathbf{x}}_{s,q}(t). \tag{4}$$

It is, otherwise, set to 0 in the former case, and to $P_{PTO,MAX}$ in the latter. The average power per sea state $\bar{P}_s$ is then obtained by averaging over the 10 considered realisations of the same sea state, and integrating over the maximal non-repeating time series $t_N \approx 2\pi/\Delta\omega$. In practice this is implemented applying the trapezoidal rule as follows.

$$\bar{P}_s = \frac{1}{10}\sum_{q=1}^{10}\frac{\Delta t}{t_N}\left(\frac{1}{2}P_{U,s,q}(t_1) + \sum_{j=2}^{j=N-1}P_{U,s,q}(t_j) + \frac{1}{2}P_{U,s,q}(t_N)\right), \tag{5}$$

with N time steps of $\Delta t = 0.05$ s. The average power per sea state is then compared to the maximum power that can be extracted by an axisymmetric device at deep waters, based on the maximum capture width CW_{MAX} and the power per metre crest width P_{pm}. This is considered to represent an upper bound,

despite the optimised shapes not being axisymmetric. The considered constraints are summarised below:

$$x_{\mathrm{MAX}}(i) = 5\mathrm{m} \quad | i = 1,3$$
$$x_{\mathrm{MIN}}(i) = -x_{\mathrm{MAX}}(i) \quad | i = 1,3$$
$$P_{\mathrm{PTO,MAX}} = 2.5\ \mathrm{MW}$$
$$0\ \mathrm{MW} \leq \bar{P}_s \leq \mathrm{CW}_{\mathrm{MAX}} \cdot P_{\mathrm{pm}}$$

The overall mean annual power is then obtained by considering the occurrence probability of each sea state O_s, so that

$$\bar{P} = \sum_{s=1}^{n_s} \bar{P}_s \cdot O_s. \tag{6}$$

2.3.2 | PTO force estimation

Based on the previously introduced assumption of a PTO semi-optimal control, the PTO-force is defined by the complex conjugate of the impedance $\mathbf{Z}^*$ as

$$\begin{aligned}\hat{\mathbf{F}}_{\mathrm{PTO}} &= -\mathbf{Z}\hat{\mathbf{U}} = -\mathbf{Z}i\omega\hat{\mathbf{X}} \\ &= [-\omega^2(\mathbf{M} + \mathbf{M}_{\mathrm{rad}}(\omega_{\mathrm{e}})) - i\omega(\mathbf{C}_{\mathrm{rad}}(\omega_{\mathrm{e}}) + \mathbf{C}_{\mathrm{loss}}) \\ &\quad + \mathbf{K}_H]\hat{\mathbf{X}}.\end{aligned} \tag{7}$$

The time series of the PTO-force $F_{\mathrm{PTO}_{s,q,i}}(t)$ can then be obtained, analogous to the oscillation time series, for each sea state s and set q of random phase shifts $\psi_{s,k,q}$ from the superposition of the single harmonic force representations at each frequency ω_k. This is calculated as

$$\begin{aligned}F_{\mathrm{PTO}_{s,q,i}}(t) = \sum_{k=1}^{n_k} \Big(&\hat{F}_{\mathrm{PTO}_{s,i}}(\omega_k) \cos(\omega_k t + \psi_{s,k,q} \\ &+ \angle \hat{F}_{\mathrm{PTO}_{s,i}}(\omega_k) \Big)\end{aligned}$$
$$\text{for} \quad s = 1,..,n_s, q = 1,..,10, i = 1,...,6.$$

As discussed in [24], PTO-stroke constraints were initially considered for the calculation of the PTO force time series by setting the PTO-force to zero when the maximum stroke (5 m) was exceeded. This assumes that the end stops absorb the total stopping load. In some cases, setting the force to zero when the stroke limit is reached could favour highly oscillating shapes. In those cases, the DEL will not be a realistic representation of PTO reliability, because the end stops are not designed to be hit every 10 s. Within this optimisation process, our aim is to generate shapes with a good trade-off between large enough oscillations to maximise power production but small enough to minimise DEL. Therefore, it is not recommended to include this type of constraint when studying PTO reliability. PTO-stroke and rating constraints are, however, assumed here to calculate the average annual power as in ref. [11].

2.4 | Fatigue damage analysis

The fatigue damage analysis focused on the fatigue failure of the rod weld connecting the floater to the PTO. Fatigue failures at welded joints or corroded bolts are speculated to become a common failure mode in WECs [5] and have high technical and economic consequence. A weld failure would cause complete shutdown for the device, require repair and replacement via re-welding of salvaged parts at sea or port, and incur an estimated long duration of downtime. If spare part, technician, and vessel availability is low, or if weather bars the repair, the cost of failure has the potential to significantly increase.

After generating the force time series from 2.3.2, we converted it to stress via the PTO piston rod area, and counted the stress cycles via Rainflow counting using the MATLAB wave analysis for fatigue and oceanography (WAFO) toolbox [31]. We then used *S–N* curves to determine the cycles to failure of the weld given the selected material, the type of weld, and the magnitude of the stress cycles. We used DNV standards on fatigue design of offshore steel structures [32], specifically *S–N* Curve *D* in Table A5 for stress perpendicular to the weld, with a traverse splice in rolled sections. This curve assumes the weld is subject to seawater and has cathodic protection.

The stress cycles were binned by their amplitudes in 20 bins, as suggested by Wægter [33]. We then used the Palmgren–Miner rule to estimate the accumulated damage, or weld fatigue caused by each binned stress range for each sea state. That is, for each bin, we divide the number of cycles in that bin by the number of cycles to failure for the given stress range. The general equation to compute the stress range is given by

$$N_{\mathrm{c}} = a_{\mathrm{D}} r^{-m}, \tag{9}$$

where N_{c} is the number of cycles in a given amplitude within a stress range, r (in MPa), a_D is the intercept parameter of the *S–N* curve and is equal to 11.764*e*6, and m is the slope of the *S–N* Curve, equal to 3 for this study. We assume the rod diameter is 6 m.

The fatigue damage per sea state was determined by summing the counted cycles per stress range. That is

$$D_{\mathrm{s}} = \sum_{i=1}^{n_r} \frac{n_{\mathrm{c}}(r_i)}{N_{\mathrm{c}}(r_i)}, \tag{10}$$

where D_{s} is the fatigue damage per sea state, N_{c} is the number of stress cycles to fatigue failure at that stress range, and n_{c} is the number of counted cycles at that stress range. The number of stress ranges in a given sea state is denoted by n_{r}. Both the counted cycles and the stress ranges for those cycles were measured by the WAFO Rainflow counting algorithm.

Finally, the fatigue damage was multiplied by the probability of occurrence of each sea state and the number of sea states in the design life to obtain the fatigue damage during the life of the WEC, as follows.

$$\mathrm{DEL}_{\mathrm{cum}} = \sum_{s=1}^{n_s} D_s \cdot O_s \cdot n_{s,d} \,, \tag{11}$$

where $\mathrm{DEL}_{\mathrm{cum}}$ is the cumulative DEL, n_s is the number of sea states, O_s is the occurrence probability of each sea state, and $n_{s,d}$ is the number of sea states in the design life. In this case, the number of sea state representations in the design life is equal to the number of hours in the design life (20 years) divided by t_N.

2.5 | Optimisation method

The multi-objective optimisation problem is formulated with variable parameters describing the hull geometry. The 22 vertices' coordinates introduced in Section 2.1 make up the decision variables. The objective functions employed for this optimisation include the overall mean power described in Section 2.3, and the cumulative DEL, calculated through the fatigue analysis framework described in Section 2.4 so that

$$f_1 = -\bar{P},$$
$$f_2 = \mathrm{DEL}_{\mathrm{cum}}.$$

Objectives are formulated in the optimisation problem to be minimised, therefore, cumulative DEL is minimised (since reducing damage is preferred) and power is multiplied by -1 in the objective function to be minimised (since increasing power production is preferred).

Four case studies in total are considered, using the two geographical sites introduced in Section 2.2 and two modes of motion for power extraction (surge and heave). Power and DEL were not normalised (non-dimensionalised) in the multi-objective optimisation process since it is difficult to define what the expected limits by which to normalise would be considering the complex shapes resulting from the optimisation. That is, there is no analytical approximation of the limit values for the objective functions.

The optimisation algorithm is an elitist non-dominated sorting genetic algorithm (NSGA-II) implementation, originally developed by Deb et al. [34]. This widely used optimisation algorithm has been proven to be particularly suitable for multi-objective problems for a wide range of applications. Meta-heuristic methods, such as genetic algorithms, are particularly suitable for solving complex problems with many decision variables. They also encourage a broader search of the solution space than direct methods, which is particularly critical when working with so many continuous decision variables. The main drawback of these methods is that the global optimality of the achieved solution cannot be proven. Therefore, hereinafter when discussing "optimal solutions", we are referring to the best solution found through the optimisation algorithm. The most suitable implementation of the NSGA-II algorithm for multi-objective optimisation of WEC hull geometries when using an adaptable geometry definition was discussed in [25]. In that study, the most suitable objective functions to represent the trade-off of power performance and costs, and the most suitable problem formulation (single-objective versus multi-objective) were discussed. For the purpose of the latter, the most suitable implementation of the multi-objective optimisation was also analysed. Reliability considerations were not included in that study. The resulting preferred implementation using intermediate recombination [35] and breeder genetic algorithm mutation [35] for the recombination and mutation operators is used. This implementation uses 22 individuals (WEC hull shapes in this case) in the population, evaluated over 100 generations. Further detail on the optimisation algorithm implementation is provided by Garcia-Teruel et al. [25].

3 | RESULTS AND DISCUSSION

In this section, we separate results of the reliability-based shape optimisation into three subsections. Section 3.1 reports the achieved objective function values for the different optimisation problems. Section 3.2 discusses the resulting optimal shapes and their characteristics. Section 3.3 compares the obtained optimisation results to the previously generated results from Clark et al. [24] for the fatigue analysis of varying, hard-coded hull shapes.

3.1 | Objective function values

The multi-objective optimisation framework generated a set of optimal solutions which best fulfil the objectives of minimising cumulative DEL ($\mathrm{DEL}_{\mathrm{cum}}$) and maximising the mean overall power ($\bar{P}$). The objective function values achieved by the set of optimal solutions create Pareto fronts, depicted for the four considered cases in Figure 4. By moving along the front, the optimal solutions minimise DEL at the expense of power production, or maximise power production at the expense of DEL, but both cannot be improved at once. Therefore, all points along the front are considered "Pareto optimal," and depending on the interests of the user, the "most optimal" point will vary along this front.

Figure 4 provides insights into how optimal shapes are affected by the met-ocean conditions and the direction of motion used for power extraction. To begin, more energetic met-ocean conditions result in greater DEL and power production. Optimal shapes for the Norway site show a larger range of objective values (both power and DEL) than those for the North Sea site. These differences in objective value ranges are attributed to the difference in available resource and predominant periods at these two sites. The site in Norway can be considered a more energetic site with more sea state variability and greater peak periods, ranging from 9.48 to 13.81

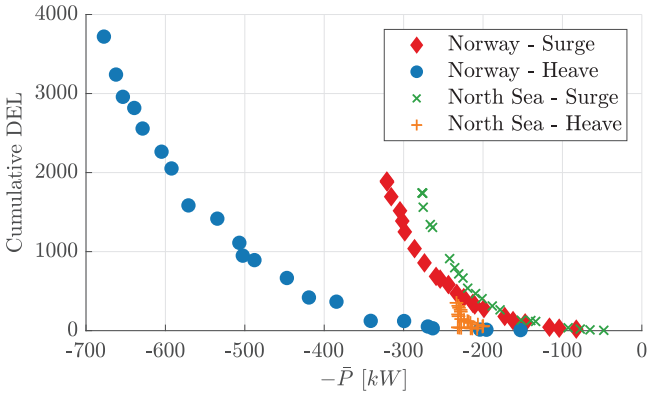

FIGURE 4 Pareto fronts for multi-objective optimisation with objective functions $-\bar{P}$ and DEL_{cum}, in the two considered locations (Norway and North Sea) and for two modes of motion (Surge and Heave)

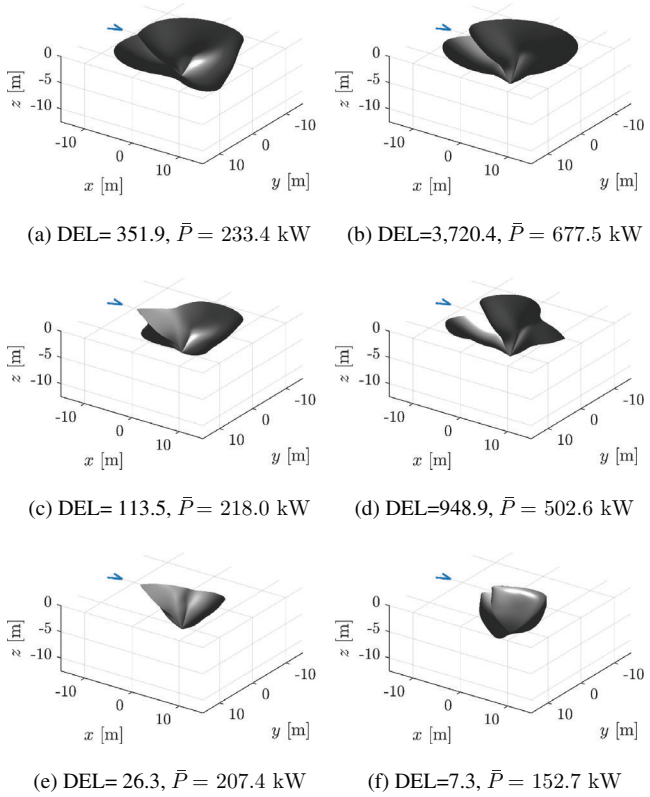

FIGURE 5 Optimal hull shapes for heaving devices from the DEL_{cum}-$\bar{P}$-Pareto front in the North Sea: (a), (c) and (e), and off the coast of Norway: (b), (d), (f). (a) and (b), and (e) and (f) are the respective Pareto front limits, and (c) and (d) are optimal geometries in the central area of each Pareto front. The DEL values provided in the captions are for DEL_{cum}

s. In comparison, the North Sea site peak periods range from 6.06 to 9.80 s. This highlights the benefit of site-specific WEC design, as well as the need for cost-oriented objectives. While this finding highlights the difference in potential structural loading and power production between sites, understanding the cost implication of these objectives would aid decision-making. For instance, the potential power production revenue and cost of repair would influence which WEC design along the Pareto front would be most optimal. If the cost of repair is high compared to the potential revenue, designs on the right side of the Pareto front would be favoured.

The influence of site-specific met-ocean conditions on objective function ranges is observed for both directions of motion (heave and surge), although it is more pronounced in the heaving WEC cases. In the Norway met-ocean conditions, the heaving WEC produces double the power of the surging WEC, and incurs 20% less DEL. Similarly in North Sea conditions, the heaving WEC produces a similar range of power, but with significantly less DEL incurred. Direction of motion, however, does affect the "Pareto point" location along the front. Both Pareto fronts for the heave cases have a more gradual curve than their surge counterparts. This results in the heave cases having greater "payoff". That is, the heave cases continue to increase power production even as DEL increases, while the surge cases incur much greater DEL for little power improvement past a certain point. This suggests that it might be advantageous to design a heaving WEC to withstand greater DEL for enhanced power production, depending on the cost of that reliability and power production revenue. Meanwhile, a surging WEC can be designed to withstand lower DELs with little loss in potential power production.

3.2 | Resulting optimal shapes

Each combination of objective values, as previously shown in the Pareto front, is achieved by one solution—a WEC hull geometry described through a unique combination of values for the 22 decision variables. When considering resulting optimal hull shapes, the shapes are more similar among the type of motion (heave and surge) than the site-specific wave conditions (North Sea and Norway). Therefore, the discussion of the resulting optimal hull geometries is divided by the direction of motion for power extraction.

3.2.1 | Heave motion

Figure 5 shows three optimal hull shapes for the solution that has the lowest DEL objective, the solution that has the greatest power objective, and the Pareto point which optimally balances the two objectives in the North Sea met-ocean conditions (Figures 5(a,c,e)) and the Norway site met-ocean conditions (Figure 5(b,d,f)). The perspective of these figures is from a point below the free surface. Note that only the submerged hull is shown in this figure. The shape above the water plane is not depicted.

There are two major characteristics that can be seen from the optimal shapes between the two sites. First, the size of the device is inversely related to the DEL objective, and positively related to the power production objective. Larger devices produce more power, but experience greater DELs (Figures 5a, 5b). Smaller devices, inversely, avoid damage but produce less power.

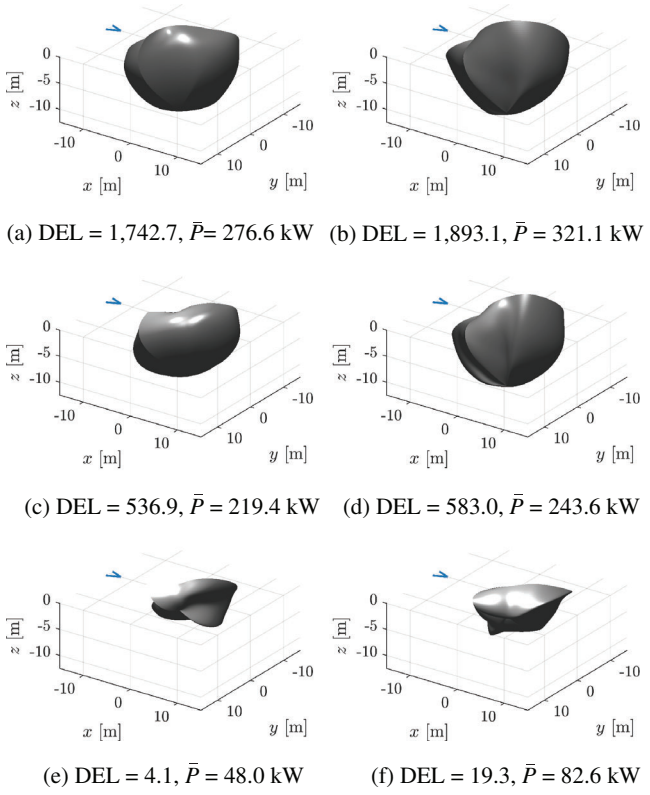

(a) DEL = 1,742.7, $\bar{P}$= 276.6 kW (b) DEL = 1,893.1, $\bar{P}$ = 321.1 kW

(c) DEL = 536.9, $\bar{P}$ = 219.4 kW (d) DEL = 583.0, $\bar{P}$ = 243.6 kW

(e) DEL = 4.1, $\bar{P}$ = 48.0 kW (f) DEL = 19.3, $\bar{P}$ = 82.6 kW

FIGURE 6 Optimal hull shapes for surging devices from the DEL_{cum}-$\bar{P}$-Pareto front in the North Sea: (a), (c), and (e), and off the coast of Norway: (b), (d), and (f). (a) and (b), and (e) and (f) are the respective Pareto front limits, and (b) and (c) are optimal geometries in the central area of each Pareto front. The DEL values provided in the captions are for DEL_{cum}

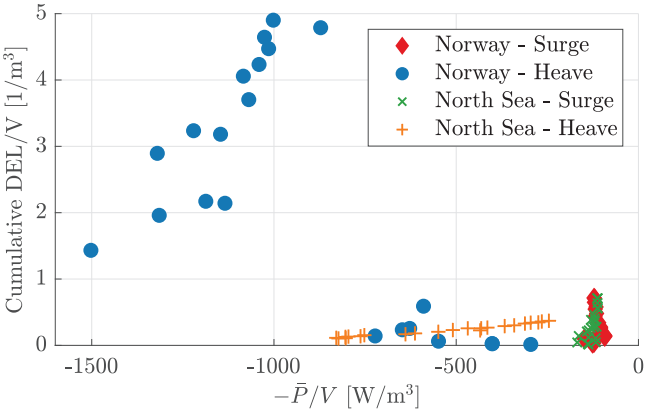

(a) Normalised by submerged volume V

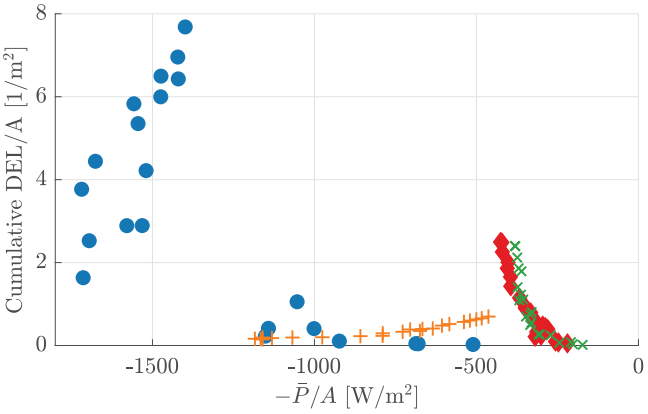

(b) Normalised by submerged surface area A

FIGURE 7 Pareto fronts $\bar{P}$ and DEL_{cum} normalised by submerged volume and submerged surface area

The Pareto optimal WEC shape, therefore, is medium-sized. Second, the shape of the hull tends to a streamlined or conical shape as the DEL_{cum} decreases. This is thought to be related to the heave motion. A larger, more convex shape achieves a greater hull volume, buoyant force, and thus power. A smaller, more concave shape reduces the loading in the heave motion. Overall, the orientation of pointed features of the WEC towards the oncoming wave direction and in the direction of motion, especially evident in Figure 5(c,e), are thought to be driven by the DEL objective, reducing surface area for oncoming waves so as to reduce loads. The larger surface area perpendicular to the heaving motion at the water plane is driven by the power objective, as discussed in [11, 25].

3.2.2 | Surge motion

The hull geometries that are optimised for surging motion are shown in Figure 6. It is observed that these hull geometries are larger and more convex than their heaving counterparts (as seen in Figure 6(c,d). Compared to the heaving case, where shapes minimise DEL with their streamlined bottoms, the geometries which minimise DEL in the surging cases have ridges facing the direction of motion - in this case becoming streamlined along the x-axis as the DEL_{cum} values reduce. This is thought to decrease the loads by minimising the surface area in this direction. Figure 6(a–d) show that in hull geometries with increased power objective values, there are less of these features, and more convex shapes. This is thought to be due to the ability to increase power by increasing the surface perpendicular to the surging direction. This is achieved through larger more convex shapes for designs with higher power production, while designs with lower DEL tend to be more streamlined with lower draft.

3.3 | Objective function values normalised by size

Differences in volume between various WEC designs were found to make comparisons of mean overall power and cumulative DEL difficult [24]. Further research by Garcia-Teruel et al. in [25, 36] identifies submerged surface area as more suitable for evaluating complex shapes than submerged volume as a proxy for costs. Therefore, the objective values for the obtained optimal shapes were normalised by the shapes' submerged volume and submerged surface area to further investigate the effects of shape and size on the results. The normalised objective values are shown in Figure 7.

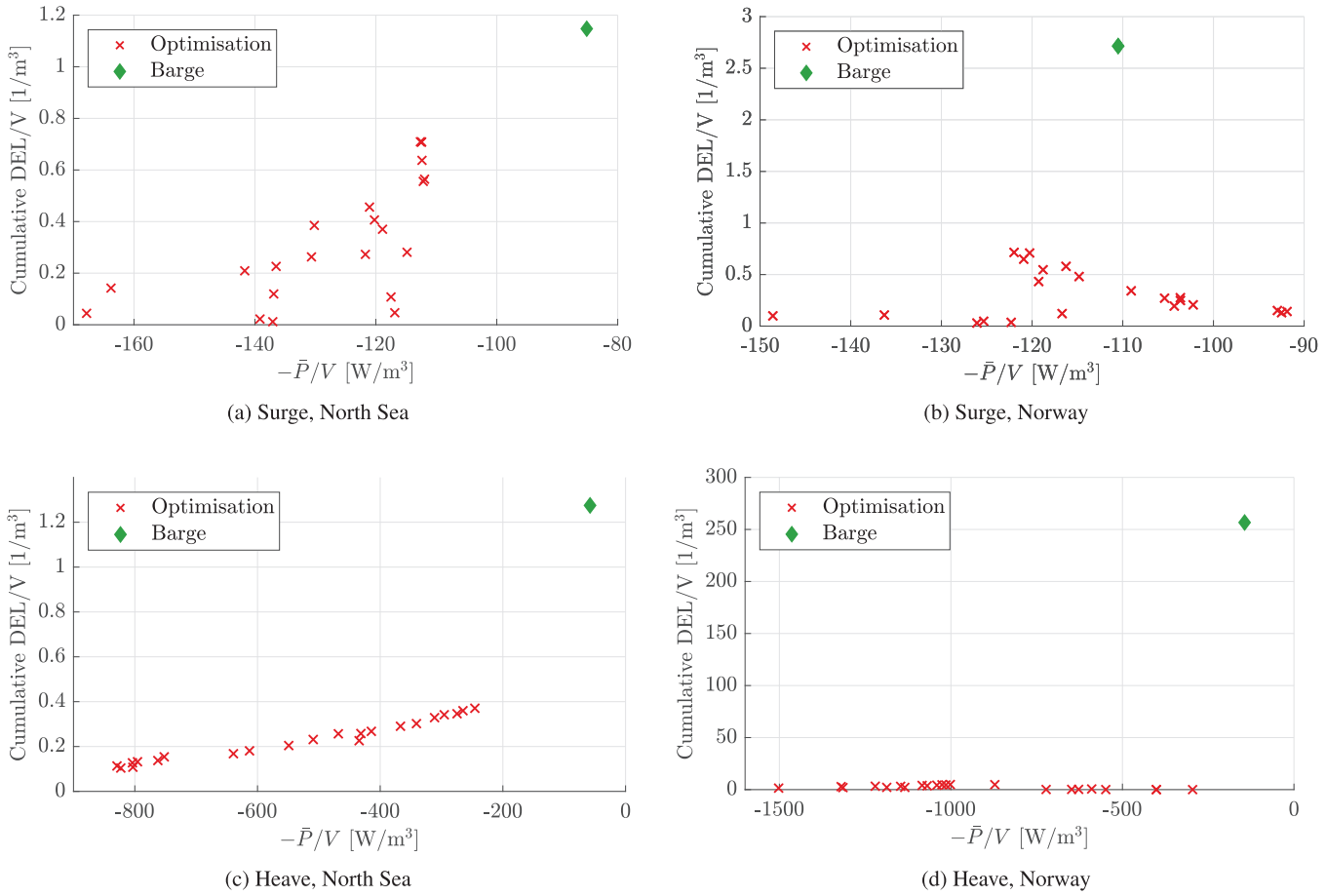

(a) Surge, North Sea

(b) Surge, Norway

(c) Heave, North Sea

(d) Heave, Norway

FIGURE 8 Pareto front $\bar{P}$ and DEL_{cum} normalised by submerged volume V for comparison with previously obtained results for hard-coded barge shape

As seen in Figure 7, the relationship between mean overall power and DEL normalised by submerged surface area and volume remains consistent with non-normalised values in the surging cases. This could indicate that, in this case, size impacts power, and DEL in a similar way. As stated before, larger devices in this case result in larger power and DEL values. In the heaving cases, however, a significant difference in the shape of the Pareto front is observed after normalising the objective values. For the North Sea cases, the relationship between DEL and power is inverted pre-normalisation. After normalisation, shapes with lower power also result in higher DELs. For the solutions found in Norway, two distinct groups of solutions can be observed. At lower power and DELs, the shape of the Pareto front is approximately maintained. However, at higher DEL and power values, the shape of the Pareto front is inverted. This could be an indicator that, for heaving cases at the Norway site, the size of the device results in larger DELs but not necessarily higher power values. If true, the shape, rather than the size, drives the power values after a certain minimum size is achieved. This is thought to be due to the waterplane surface area value being the main driver for power extraction in heave, and large waterplane surface area values not having a strong impact on the device's submerged volume and surface area. Once the maximum waterplane area is achieved, further increases in volume may not result in increases in power, but may result in increases in DEL.

To verify the value of the multi-objective optimisation process compared to non-optimised shapes, the results obtained for the optimal shapes generated through this process are compared to the results obtained for a barge of predefined dimensions in a previous study [24]. Although width (20 m) and draft (10 m) dimensions of the barge are comparable to the geometric constraints used to generate the more complex optimal shapes, volumes vary largely across shapes. To allow for a fairer comparison, the submerged volume normalised objectives are used. The normalised objectives for the optimised and the hard-coded barge shapes are shown in Figure 8.

As seen in Figure 8, most cases show the optimised shapes result in a significantly better trade-off of mean overall power and cumulative DEL when normalised with their submerged volume. This shows, that both utilising design optimisation to generate improved solutions and using adaptable geometry definitions within a WEC hull design optimisation process can provide valuable insights regarding optimal geometry features, that may not become apparent if employing simple shapes.

To improve the behaviour of the optimisation algorithm further in the future, it is recommended to seed the initial population in the optimisation algorithm with high-performing shapes

from across the solution space, resulting in faster convergence, greater exploration of the solution space, and avoidance of local minima.

3.4 | Assumptions and limitations

This study is based on linear wave theory and therefore only small oscillations are considered. That implies that nonlinear effects such as nonlinear Froude–Krylov forces and viscous damping are not considered. Efficient methods for nonlinear Froude–Krylov modelling have been proposed for axisymmetric bodies in [37]. However, for the present case, where non-axisymmetric geometries are considered nonlinear models would be computationally inhibitive when part of an optimisation process. Additionally, the hydrodynamics are modelled using a frequency-domain method, precluding the consideration of non-linear effects from a real PTO or mooring system, for example. In future work, this shortcoming could be addressed by applying a time-domain model, although it would be significantly more computationally expensive. Therefore, a detailed comparison of different hydrodynamic models and their impact on the resulting optimal shapes should be performed in the future to determine the best trade-off between model accuracy and computational time for early-stage WEC design optimisation.

In this study, we assume uni-directional wave cases and that the WEC is always aligned with respect to the oncoming wave direction. This was the chosen approach because the joint environmental data used in this study does not account for wave direction, assuming wind and wave conditions are collinear and uni-directional. However, multi-directional wave conditions would have an impact on PTO reliability, and therefore resulting optimal shapes. The inclusion of multi-directional wave conditions could be included through BEM simulations of the WEC in future work, but managing computational expense so that the problem remains tenable will become paramount. Optimising for shape renders many computational load estimation shortcuts (for example, surrogate modelling) ineffective. Thus, novel ways to reduce computational time while improving realistic load simulation are needed.

The fact that the optimisation functions are not normalised (non-dimensionalised), means that the different objective functions may have different weight on the optimal solutions. However, as discussed in the results, interesting insights were gained regarding the weight of the objective functions when normalising the objectives by submerged surface area and submerged volume. In this study, results from a DEL-only versus a power-only objective were presented to gain a better understanding of the impact of each objective function on the resulting optimal shapes. In the future, when generating shapes that minimise the overall levelised cost of energy, submerged surface area, or volume can be included as cost proxies in the objective functions.

For further analysis, more advanced modelling techniques to account for nonlinear dynamics, more complex wave condition considerations, and objective function variants can be integrated now that the Pareto front of preliminary designs is obtained. The generated Pareto optimal set enables further research by identifying the most suitable designs for further more detailed assessment and development.

3.5 | Summary

Collectively, these results indicate that geometry, size, as well as direction of motion and siting are all important factors in reducing PTO cumulative DELs. Geometry, both overall shape (e.g. spherical, conical) and particular geometrical features (concavity, convexity, and pointed or edged features) affect DEL and power. When extracting power via the surge motion, increased size and convexity result in increased power production, whereas smaller sizes streamlined in the surging direction produce minimised DELs. When extracting power via the heave motion, concave, streamlined shapes in the heaving direction resulted in lower DELs. Heaving WECs have more variability in power production, especially across sites. Surging WECs have less variability in power produced (even across sites). Both heaving and surging cases experience more variability in DEL and power in the Norway site than the North Sea site, indicating that sea state conditions are an important factor in optimal design of WECs.

4 | CONCLUSIONS

In this study, we explore the relationship between WEC floater hull geometry and PTO reliability. We build on a preliminary study [24] in which we analysed twelve fixed-geometry cases, across two locations (North Sea and Norway), two modes of motion (heave and surge), and three shapes (barge, cylinder, and sphere) - to develop a method by which to integrate reliability assessment into a shape optimisation process. In this method, DEL on the rod weld connecting the WEC floater to the PTO is calculated. The fatigue analysis and power calculation methods established for the fixed-geometry cases are then enveloped in a multi-objective genetic algorithm to optimise variable WEC hull geometries for power production and PTO reliability.

Results indicate a clear dependence of cumulative DELs on location, power extraction direction (heave versus surge), size, and geometry. Therefore, it is critical to consider all these parameters in the early design of WECs for optimal performance. This study highlights the benefit of incorporating reliability objectives into early WEC design simultaneously with power production, rather than secondary to them. Developing a reliability-based optimisation framework for WECs enables developers and researchers to incorporate reliability considerations in early design phases. This allows them to explore the trade-off between power production, cost and reliability objectives, prior to costly redesign or failure, therefore, advancing the techno-economic feasibility of this technology. Furthermore, this study indicates an opportunity for greater device performance and reliability through site-specific design.

Much like the wind energy industry has adapted to a development model in which device developers choose turbine models based on the site and resource conditions, the wave energy industry could benefit from developing WECs based on the energy density, water depth, or other characteristics of the site and resource. Efforts to create standards for wave energy resources and WECs that mimic wind energy resource and turbine classifications exist [38], but probabilistic design [39] of WECs could further accelerate advanced WEC design and promote a more thorough inclusion of performance and loads.

In future work, the method used to characterise PTO reliability should be enhanced with a more advanced PTO model. In particular, including more realistic PTO dynamics and stroke constraints is recommended. This would enable an enhanced PTO force and reliability analysis to be included in the optimisation framework. To achieve this, the use of a more detailed representation of the hydrodynamics should be further investigated, for example, by considering multi-directional waves and time-domain models. Additionally, while this study serves as the basis for reliability-based design optimisation work, future work to incorporate power production revenue and operations and maintenance cost models would enable us to better understand the financial balance between reliability and power production. This ability to consider optimal designs along a Pareto front in terms of cost would enable developers to create enhanced designs, incorporating reliability, power, and cost into WEC hull design, and explore the unique optimal sets that exist for different power extraction motions and site conditions.

ACKNOWLEDGMENTS

The authors would like to thank the International Network on Offshore Renewable Energy (INORE) for supporting this work with a Blue Energy Collaborative Scholarship (BECS) sponsored by Ocean Energy Systems (OES).

ORCID

Anna Garcia-Teruel https://orcid.org/0000-0002-2121-9250
Caitlyn E. Clark https://orcid.org/0000-0002-5203-7329

REFERENCES

1. IEA-OES: Blue economy and its promising markets for ocean energy. IEA Technology Collaboration Programme for Ocean Energy Systems (OES), (2020) www.ocean-energy-systems.org. Accessed 21 June 2021
2. Hodges, J. et al.: An international evaluation and guidance framework for ocean energy technology. IEA Technology Collaboration Programme for Ocean Energy Systems (OES), (2021). https://www.ocean-energy-systems.org/documents/47763-evaluation-guidance-ocean-energy-technologies2.pdf/. Accessed 21 June 2021
3. Coe, R., Yu, Y.H., van Rij, J.: A survey of WEC reliability, survival and design practices. Energies 11(1), 4 (2017)
4. Clark, C.E., DuPont, B.: Reliability-based design optimization in offshore renewable energy systems. Renew. Sustain. Energy Rev. 97, 390–400 (2018)
5. Ambühl, S., Kramer, M., Sørensen, J.D.: Reliability-based structural optimization of wave energy converters. Energies 7, 8178–8200 (2014)
6. Ambuhl, S.: Reliability of wave energy converters, (2015) https://www.riverpublishers.com/pdf/ebook/RP_978-87-93379-05-3.pdf. Accessed 21 June 2021
7. Wolfram, J.: On assessing the reliability and availability of marine energy converters: the problems of a new technology. Risk and Reliability 220(1), 55–68 (2006)
8. Garcia-Teruel, A., Forehand, D.I.M.: A review of geometry optimisation of wave energy converters. Renewable Sustainable Energy Rev. 139, 110593 (2021)
9. McCabe, A.P., Aggidis, G.A., Widden, M.B.: Optimizing the shape of a surge-and-pitch wave energy collector using a genetic algorithm. Renewable Energy 35(12), 2767–2775 (2010)
10. McCabe, A.P.: Constrained optimization of the shape of a wave energy collector by genetic algorithm. Renewable Energy 51, 274–284 (2013)
11. Garcia-Teruel, A., Forehand, D.: Optimal wave energy converter geometry for different modes of motion. In: Advances in Renewable Energies Offshore Proc. 3rd Int. Conf. Renew. Energies Offshore (RENEW 2018), pp. 299–305. CRC Press, Boca Raton, FL (2018)
12. Garcia-Teruel, A., DuPont, B., Forehand, D.I.M.: Hull geometry optimisation of wave energy converters: On the choice of the optimisation algorithm and the geometry definition. Appl. Energy 280, 115952 (2020)
13. Kurniawan, A., Moan, T.: Optimal geometries for wave absorbers oscillating about a fixed axis. IEEE J. Ocean Eng. 38(1), 117–130 (2013)
14. Ambühl, S. et al.: Reliability assessment of wave energy devices. In: 11th International Conference on Structural Safety and Reliability. Aalborg University, Aalborg (2013)
15. Yang, L.M., Hals, T., Moan, T.: A wear model for assessing the reliability of wave energy converter in heave with hydraulic power take-off. In: Proc. 8th European Wave Tidal Energy Conf, pp. 874–881. Tethys, Washington, DC (2009)
16. Tom, N. et al.: Preliminary analysis of an oscillating surge wave energy converter with controlled geometry. In: European Wave and Tidal Energy Conference, pp. 1–10. Golden, CO (2015)
17. Yu, Y.H. et al.: Design and analysis for a floating oscillating surge wave energy converter. In: Proc. of 33rd International Conference on Ocean, Offshore and Arctic Engineering (OMAE), pp. 1–7. ASME, New York (2014)
18. Beirão, P.J.B.F.N., dos Santos Pereira Malça, C.M.: Design and analysis of buoy geometries for a wave energy converter. Int. J. Energy Environ. Eng. 5(2–3), 91 (2014)
19. Yu, Y.H. et al.: Preliminary wave energy converters extreme load analysis. In: Proc. of the 34th International Conference on Ocean, Offshore and Arctic Engineering (OMAE), pp. 1–7. ASME, New York (2015)
20. van Rij, J., Yu, Y.H., Guo, Y.: Structural loads analysis for wave energy converters. In: Proc. of the 36th International Conference on Ocean, Offshore and Arctic Engineering (OMAE), pp. 1–9. ASME, New York (2017)
21. van Rij, J., Yu, Y.H., Coe, R.G.: Design load analysis for wave energy converters. In: Proc. of the 37th International Conference on Ocean, Offshore and Arctic Engineering (OMAE), pp. 1–10. ASME, New York (2018)
22. van Rij, J., et al.: Ocean power technology design optimization. Int. J. Mar. Energy 20, 97–108 (2017)
23. NREL, Sandia: WEC-Sim (Wave Energy Converter SIMulator) – WEC-Sim documentation, (2020). https://wec-sim.github.io/WEC-Sim/. Accessed 21 June 2021
24. Clark, C.E. et al.: Towards reliability-based geometry optimization of a point-absorber with PTO reliability objectives. Paper presented at Proc. of 13th European Wave and Tidal Energy Conference (EWTEC), Naples, 1–6 Sept 2019
25. Garcia-Teruel, A., DuPont, B., Forehand, D.I.M.: Hull geometry optimisation of wave energy converters: On the choice of the objective function and the optimisation formulation. Appl. Energy 298, 117153 (2021)
26. Garcia-Teruel, A., DuPont, B., Forehand, D.I.M.: Hull geometry optimisation of wave energy converters: On the choice of the optimisation algorithm and the geometry definition. figshare (2020) https://doi.org/10.6084/m9.figshare.13070234.v1. Accessed 21 June 2021
27. Sojo Armentia, M., Auer, G.: MARINA Platform Final Summary Report. (2014) https://cordis.europa.eu/project/id/241402/reporting. Accessed 21 June 2021
28. Li, L., Gao, Z., Moan, T.: Joint environmental data at five european offshore sites for design of combined wind and wave energy

devices. In: ASME 2013 32nd International Conference on Ocean, Offshore and Arctic Engineering. vol. 8. (2013). https://doi.org/10.1115/OMAE2013-10156
29. MIT: WAMIT User Manual (2016). http://www.wamit.com/manualupdate/V70_manual.pdf. Accessed 10 February 2016
30. Babarit, A., et al.: Numerical benchmarking study of a selection of wave energy converters. Renew Energy 41, 44–63 (2012)
31. The WAFO Group: WAFO–a Matlab toolbox for analysis of random waves and loads. Lund University, Lund (2011). http://www.maths.lth.se/matstat/wafo/documentation/wafoiso.ps. Accessed 1 August 2019
32. DNV: RP-C203- Fatigue design of offshore steel structures. Recommended Practice DNV-RPC203 (2014). ftp://128.84.241.91/tmp/MSE-4020/Fatigue-Design-Offshore.pdf
33. Waegter, J.: Stress range histories and rain flow counting. pp. 1–13. Aalborg University (2009) http://homes.civil.aau.dk/lda/Advanced%20Structural%20Engineering/Stress%20range%20histories%20and%20Rain%20Flowcounting.pdf. Accessed 21 June 2021
34. Deb, K. et al.: A fast elitist non-dominated sorting genetic algorithm for multi-objective optimization : NSGA-II. In: Proc of the 6th International Conference on Parallel Problem Solving from Nature (PPSN VI), pp. 1–11. Springer-Verlag, London (2000)
35. Mühlenbein, H., Schlierkamp-Voosen, D.: Predictive models for the breeder genetic algorithm. Evol. Comput. 1(1), 25–49 (1993)
36. Garcia-Teruel, A., Forehand, D.I.M., Jeffrey, H.: Metrics for wave energy converter hull geometry optimisation. Paper presented at Proc. of the 13th European Wave and Tidal Energy Conference (EWTEC), Naples, 1–6 Sept 2019
37. Giorgi, G., Ringwood, J.V.: Computationally efficient nonlinear Froude – Krylov force calculations for heaving axisymmetric wave energy point absorbers. Journal of Ocean Engineering and Marine Energy 3(1), 21–33 (2017)
38. Neary, V.S. et al.: Classification systems for wave energy resources and WEC technologies. In: Proc. of the 12th European Wave and Tidal Energy Conference, vol. 973, pp. 1–9. EWTEC, Cork (2017)
39. Sørensen, J.D., Toft, H.S.: Probabilistic design of wind turbines. Energies 3(2), 241–257 (2010)

How to cite this article: Garcia-Teruel, A., Clark, C.E.: Reliability-based hull geometry optimisation of a point-absorber wave energy converter with power take-off structural reliability objectives. IET Renew. Power Gener. 1–14 (2021). https://doi.org/10.1049/rpg2.12249

APPENDIX A

TABLE A.1 Characteristic sea sates for Site 15 (North Sea)

Sea State	H_s [m]	T_p (s)	Prob. (%)	Occ./year (hrs)
1	0.64	6.06	13.1	1145
2	0.73	6.13	8	698.2
3	0.77	6.17	2.1	186.2
4	0.8	6.19	0.3	27.9
5	1.26	6.55	5.8	512
6	1.43	6.68	17.3	1517.4
7	1.56	6.78	13.2	1154.3
8	1.63	6.83	3.9	344.4
9	1.66	6.86	0.6	55.9
10	1.69	6.88	0.1	9.3
11	2.22	7.28	1.9	167.6
12	2.37	7.4	9.5	828.5
13	2.51	7.5	8.5	744.7
14	2.58	7.56	2.6	223.4
15	2.61	7.58	0.3	27.9
16	3.21	8.05	0.6	55.9
17	3.35	8.16	3.9	344.4
18	3.48	8.26	3.5	307.2
19	3.55	8.32	1	83.8
20	3.59	8.35	0.1	9.3
21	4.21	8.85	0.2	18.6
22	4.35	8.96	1.4	121.09
23	4.47	9.06	1.1	93.1
24	4.54	9.11	0.2	18.6
25	5.22	9.68	0.1	9.3
26	5.36	9.8	0.4	37.2
27	5.47	9.89	0.2	18.6
			99.9	**8815.6**

TABLE A.2 Characteristic sea states for Site 14 (Norway)

Sea state	H_s [m]	T_p (s)	Prob. (%)	Occ./year (hrs)
1	0.67	9.48	3.3	282.2
2	0.70	9.51	3.9	335.0
3	0.73	9.55	1.1	92.7
4	0.77	9.59	0.1	9.5
5	1.50	10.30	7.2	615.9
6	1.54	10.33	12.5	1070.4
7	1.58	10.36	5.6	479.2
8	1.62	10.39	0.9	79.2
9	1.65	10.41	0.1	5.4
10	2.42	10.94	4.4	374.7
11	2.46	10.96	12.1	1035.5
12	2.51	10.99	9.4	806.9
13	2.56	11.02	2.5	212.9
14	2.59	11.04	0.2	21.3
15	3.35	11.46	1.1	93.7
16	3.40	11.48	5.3	541.4
17	3.46	11.51	8.2	699.5
18	3.52	11.54	3.8	327.5
19	3.56	11.56	0.6	49.4
20	4.30	11.91	0.1	10.1
21	4.34	11.93	1.1	92.2
22	4.41	11.96	3.8	326.4
23	4.48	11.99	3.7	315.4
24	4.53	12.01	0.9	479.8
25	4.56	12.03	0.1	6.4
26	5.29	12.33	0.1	8.6
27	5.36	12.36	0.9	78.9
28	5.43	12.39	2.2	185.5
29	5.50	12.42	1.1	91.7
30	5.54	12.44	0.1	11.3
31	6.30	12.73	0.1	9.3
32	6.38	12.76	0.7	62.4
33	6.46	12.79	0.8	72.0
34	6.52	12.81	0.2	15.6
35	7.33	13.11	0.1	11.0
36	7.42	13.14	0.4	36.0
37	7.49	13.16	0.2	16.3
38	8.37	13.46	0.1	10.4
39	8.46	13.49	0.1	12.1
40	9.42	13.81	0.1	5.9
			99.5	**8499.5**